Site Specific Seismic Performance of Circular Tunnels in Dry Sand

F. de Silva[1,2(✉)], S. Fabozzi[2], N. Nikitas[3], E. Bilotta[1], and R. Fuentes[3]

[1] Department of Civil Architectural and Environmental Engineering (DICEA), University of Naples Federico II, via Claudio 21, 80125 Naples, Italy
filomena.desilva@unina.it
[2] Istituto di Geologia Ambientale e Geoingegneria, Consiglio Nazionale delle Ricerche, Area della Ricerca Roma 1, via Salaria km 29300, 00015 Monterotondo, Rome, Italy
[3] School of Civil Engineering, University of Leeds, Woodhouse Lane, Leeds LS2 9JT, UK

Abstract. Past earthquakes revealed that underground tunnel structures are exposed to seismic risk and their seismic vulnerability is mainly function of the tunnel structure technology, the soil-tunnel interaction developing during the seismic shaking and the intensity of the seismic event. Each of these factors plays an important role in terms of the probability of damage and loss of functionality due to the tunnel deformations induced by increments in internal forces. Currently, the fragility curves are among the most widespread methods for the rapid assessment of structural performance at different hazard levels, giving the probability of reaching a defined damage level with respect to a given level of seismic motion. In the present work, a recently developed approach to evaluate the seismic risk has been applied to circular tunnels, whereby the main focus is the expression of the failure annual rate through the convolution of the fragility of the system under investigation and the seismic hazard on site. In this way, a direct link between the performance of the structure with its measuring parameter is established. The procedure has been adopted for some reference tunnel sections of the Metro Line of Naples.

Keywords: Seismic risk · Seismic hazard · Fragility curves · Tunnel lining · 2D FDM

1 Introduction

Many existing studies on seismic performance-based assessment of tunnels or underground cavities (Salmon et al. 2003; Argyroudis and Pitilakis 2012; Andreotti and Lai 2014; Pitilakis et al. 2014; Kiani et al. 2016; Argyroudis et al. 2017; Fabozzi et al. 2017; de Silva and Scotto di Santolo 2018) were aimed to individuate the damage under specific earthquake scenarios or the fragility of the system under weak to strong earthquakes.

One of the most recent developments of performance-based earthquake engineering is the expression of the failure annual rate, obtained from the convolution of the

F. Calvetti et al. (Eds.): CNRIG 2019, LNCE 40, pp. 537–544, 2020.
https://doi.org/10.1007/978-3-030-21359-6_57

fragility of the system under investigation and the seismic hazard on site. The approach is considered state-of-the-art in terms of assessing the seismic risk of structures (Jalayer and Cornell 2009; Iervolino et al. 2017), while few pioneering applications have been developed by geotechnical researchers (Kramer 2008, 2014).

In this study, the approach is applied to estimate the seismic risk of underground tunnel sections, under different subsoil conditions, in Naples. The site-specific hazard curve was combined with fragility curves generated from the results of nonlinear dynamic analyses of the soil-tunnel system.

2 Method of Analysis

Once the failure mechanism of the analysed structure is selected, its seismic performance is conventionally quantified through the demand to capacity ratio, DCR. For a given intensity measure, IM, of the input motion, the DCR is usually log-normally distributed and the relationship between the mean DCR and the IM is nearly linear in a log-log plot, governed by the fitting parameters a and b as shown in Fig. 1b. Under these hypotheses, the probability of the DCR exceeding a specific value y, i.e. the fragility, is computed as in Eq. 1:

$$P(DCR > y|IM) = 1 - \Phi\left(\frac{\log(y) - \log\eta_{DCR|IM}}{\sigma}\right) \quad (1)$$

where σ is the logarithmic standard deviation for the DCR given the IM and the associated mean is given by Eq. 2:

$$\log\eta_{DCR|IM} = \log(a) + b\,\log(IM) \quad (2)$$

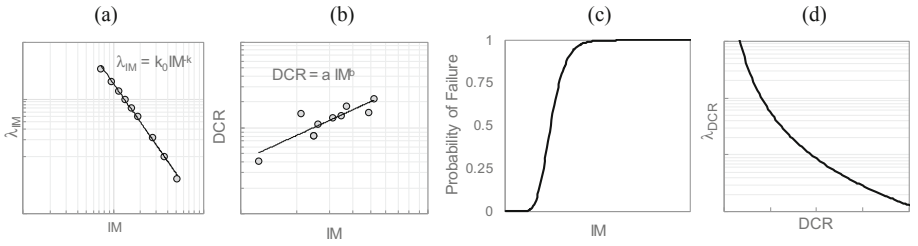

Fig. 1. Main steps of the adopted method: power law model fitting hazard curve (a) and DCR-IM relationship (b), fragility curve (c) and DCR hazard curve (d).

Obviously, the mobilization of the capacity is strictly influenced by the exciting input motion, i.e. by the on-site hazard. This aspect is taken into account by the convolution of the site-specific hazard curve λ_{IM} in Fig. 1a with the aforementioned

fragility curve of the analysed system (Fig. 1c), to compute the annual rate of exceeding a performance level (Eq. 3):

$$\lambda_{DCR} = \int_0^{+\infty} P(DCR > y|IM) \cdot |d\lambda_{IM}(x)| \quad (3)$$

In Eq. 3, the absolute value of the derivative of the hazard curve $|d\lambda_{IM}(x)|$ at each level of the intensity measure IM = x can be easier computed fitting the hazard curve with a power law, as shown in Fig. 1a. In most of the applications (Jalayer and Cornell 2009; Iervolino et al. 2017; Miano et al. 2018), Eq. (1) and (3) are applied for y = 1 corresponding to the failure with respect to the assumed limit state. In this study, the annual rate associated to the partial mobilization of the capacity was computed varying y in the range [0, 1], to obtain the DCR hazard curve shown in Fig. 1d.

3 Fragility Curves of Circular Tunnels in Dry Sand

The computation of fragility curves was executed based on the results of 2D nonlinear dynamic analyses performed on the following four schemes of a circular tunnel in dry sand:

- shallow tunnel in loose sand (C/D = 1, Dr = 40%, see Fig. 2a)
- shallow tunnel in dense sand (C/D = 1, Dr = 75%)
- deep tunnel in loose sand (C/D = 2.5, Dr = 40%)
- deep tunnel in dense sand (C/D = 2.5, Dr = 75%).

Figure 2a shows the numerical model generated through the FLAC code (Itasca 2011). The depth of the tunnel axis was changed from 15 m (C/D = 1) to 30 m (C/D = 2.5) and two idealized soil models were considered representative of loose and dense sand and characterized by a relative density Dr = 40% and Dr = 75%, respectively. The hysteretic elastic perfectly plastic Mohr-Coulomb constitutive model was adopted for the soil in which the shear wave velocity, V_S, increases with depth, following the empirical power law correlation by Hardin (1978). The resulting profiles were corrected close to the ground surface to avoid the unrealistic convergence to zero. The small strain shear stiffness, G_0, and bulk modulus, K_0, the soil density, ρ, Poisson ratio, ν, and the friction angle φ of the cohesionless soil are reported in Table 1. The hysteretic soil response was calibrated on the variation of the normalized shear modulus, G/G_0, and damping ratio, D, with shear strain, γ, proposed for sand by Seed and Idriss (1970).

A 10 m thick layer of soft rock was placed below the sand with a linear behaviour governed by the typical physical and mechanical properties of a seismic bedrock (see Table 1).

The lining was assumed to be 0.50 m thick and made of R_{ck} = 25/30 concrete with Young modulus E = 3000 MPa, Poisson ratio ν = 0.15 and uniaxial compression and tensile strengths σ_{cy} = 25 MPa and σ_t = 2.5 MPa, respectively. A linear elastic behavior was set for the lining during the analyses, to compute the seismic demand; the strength values were later introduced in the computation of the capacity.

Table 1. Physical and mechanical soil properties.

	ρ [kg/m^3]	Dr [%]	V_S [m/s]	G_0 [MPa]	ν [/]	K_0 [MPa]	φ [°]
Loose sand	1600	40	150–300	36–144	0.33	94–376	30
Dense sand	1800	75	230–450	95–365	0.30	206–790	35
Bedrock	2000	/	800	1024	0.15	1122	/

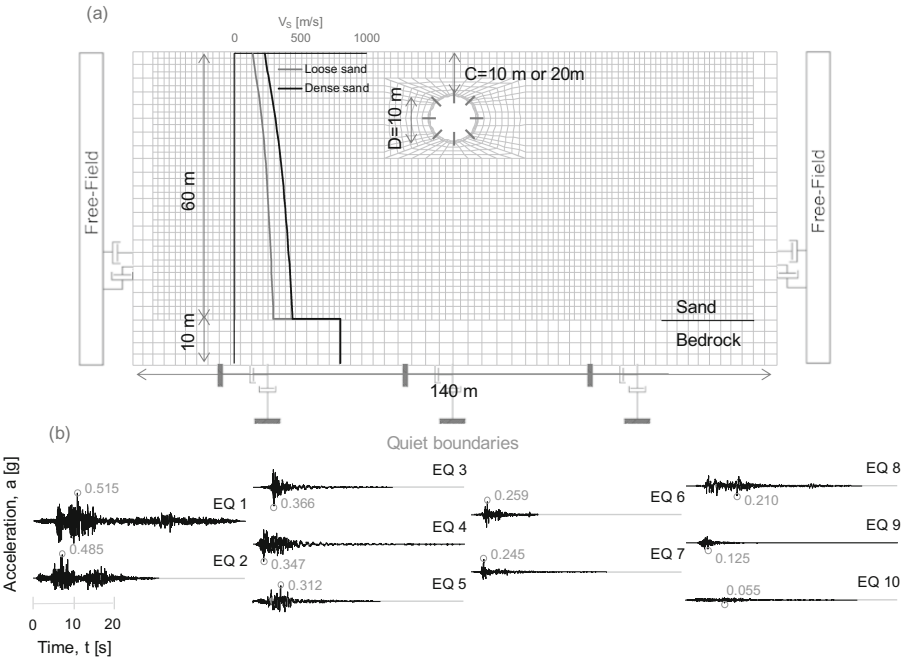

Fig. 2. Numerical model with shear wave velocity profiles (a) and input motions (b) adopted in the dynamic analyses.

The mesh size, Δ, was calibrated according to the rule $\Delta < V_S/8f_{max}$ proposed by Kuhlemeyer and Lysmer (1973), to allow for typical seismic wave frequencies up to f_{max} = 25 Hz, to reliably propagate through the layered soil. Smaller mesh elements were used to model the tunnel lining. To minimize the model size, the so-called 'free-field' boundary conditions were imposed along the lateral sides and quiet boundaries were placed at the bottom to simulate the infinite extension in depth of the bedrock.

The seismic response of each model was simulated under ten natural accelerograms selected from the PEER ground motion database (Pacific Earthquake Engineering Research center, https://ngawest2.berkeley.edu/site/documentation) with peak ground accelerations, PGA, ranging from 0.515 g to 0.055 g (see Fig. 2b).

The stresses acting on the control sections of the lining identified in Fig. 2a were recorded to compute the evolution of axial force N(t) and the bending moment, M_{load}(t), during each seismic analysis. The tunnel safety was assessed by comparing

$M_{load}(t)$ to the moment $M_{res}(t)$ associated to the reaching of the tensile strength σ_t in the concrete of the lining. This latter was computed from the equilibrium of a 1 m thick moment-resisting section reinforced with 20 Φ10 steel bars symmetrically placed at a distance 0.15 m from the centre of the section. The scheme for the calculation is shown in Fig. 3, whereby σ_c is the maximum compression stress acting on the concrete and σ_{ru} and σ_{rl} are the stresses acting on the upper and lower reinforcements, typically normalized through the steel-concrete homogenization coefficient n = 6.7. The equilibrium was calculated at each time step using a routine implemented in Matlab, to take into account the time-dependence of $M_{res}(t)$, due to the changes of the axial force during the seismic excitation. The maximum ratio between the loading and the resisting moment in the time history of each earthquake was assumed as the DCR.

Figure 3 shows the fragility curves computed through Eq. 1 for y = 1 by calibrating the parameters a, b and σ on the numerical results, as explained in Sect. 2. The scatter between the probability of failure of tunnels in dense and loose sand is associated to the different site amplifications, with high amplitudes of input motion being dampened by loose soils thereby reducing the fragility of the embedded tunnel. A more detailed discussion on the seismic soil-tunnel interaction and its effect on the safety of linear infrastructure is reported in de Silva et al. (2019).

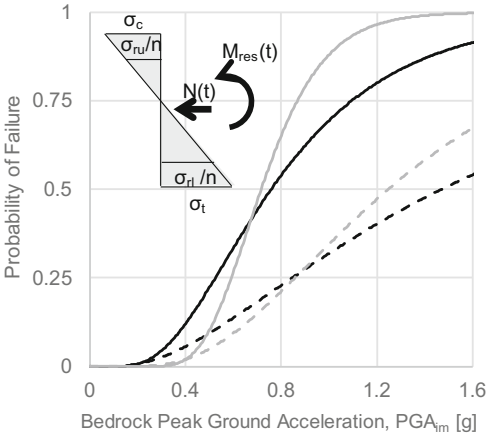

	DEEP TUNNEL		SHALLOW TUNNEL	
	dense sand	loose sand	dense sand	loose sand
a	1.51	0.73	1.41	0.83
b	1.47	0.82	1.02	0.83
σ	0.80	0.67	0.29	0.46

Fig. 3. Fragility curves of shallow and deep tunnel in dry and loose sand.

4 Seismic Hazard of the Selected Site

Different tunnel sections of the Metro Line of Naples, excavated with conventional heading excavation method, have been considered for the application of the adopted methodology, corresponding to similar subsoil conditions of the fragility curves presented in Sect. 3. The Probabilistic Seismic Hazard Analysis (PSHA) has been used to evaluate the expected seismic scenario for the selected case of study. In particular, the PGA values expected to occur on a stiff rock outcrop have been extracted from the Italian

seismic hazard database made available by the INGV (http://zonesismiche.mi.ingv.it). Figure 4a, for instance, shows the hazard map of Italy in correspondence of a probability of exceedance, p_{vr}, equal to 10% and the relative location of the site of study, while Fig. 4b plots the PGA hazard curves in correspondence of the 16°, 50° and 84° percentile computed for the coordinates of the considered site. The 50° percentile seismic hazard curve was considered in the following application (Sect. 5).

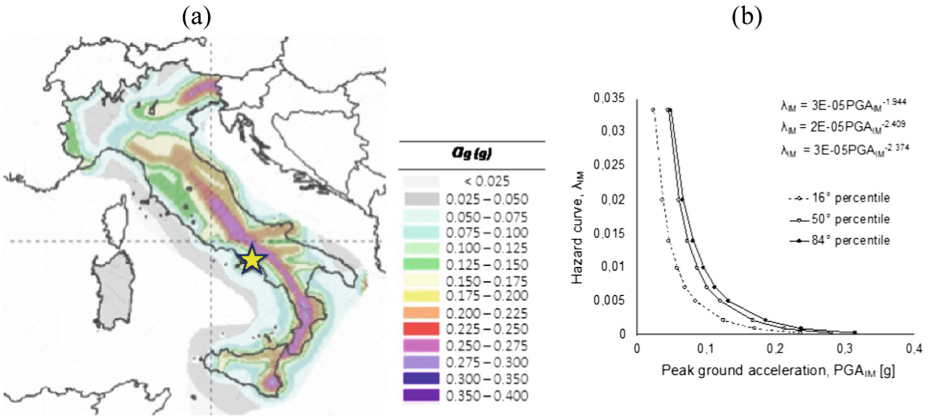

Fig. 4. PGA hazard map for a probability of exceedance, p_{vr}, equal to 10% (a) and hazard curves (b) of Naples (http://zonesismiche.mi.ingv.it).

5 Mean Annual Frequency of Exceeding the Performance Levels

Figure 5 shows the demand to capacity hazard curves obtained by combining, through Eq. 3, the hazard curve of Naples corresponding to 50° percentile with the fragility curves of the four reference schemes calculated for different performance levels. It is worth remembering that only the points associated through DCR = 1, i.e. the mean annual rate of failure, were computed through the fragility curves shown in Fig. 3. The huge difference obtained in the fragility curves between tunnels in loose and dense sand are attenuated by the convolution with the on-site hazard, since the higher values of λ_{IM} are associated to PGA < 0.2 g circa (see Fig. 4), where the fragility curves of the four models are very close together (see Fig. 3).

Assuming a reference life-time V_R = 50 years and a utilization coefficient cu = 1, the return periods T_R associated to the probability of exceedance, p_{VR}, defined by the Italian Code (NTC2018) for the limit states were computed. With $\lambda_{DCR} = 1/T_R$, the annual rate of exceeding the serviceability limit states SLO (p_{VR} = 81%) and SLD (p_{VR} = 63%) and ultimate limit states SLV (p_{VR} = 10%) and SLC (p_{VR} = 5%) were calculated. The results are overlaid within Fig. 5, highlighting that the capacity expected to be mobilized in one-year ranges from 0.1 to 0.2 for SLO and SLD, while 0.25 < DCR < 0.45 for SLV and SLC. With respect to the traditional approach, the

DCR hazard curves link directly the desired performance with its measuring parameter DCR, which is much more consistent with the definition of the limit states and in general with the rationale of performance-based design.

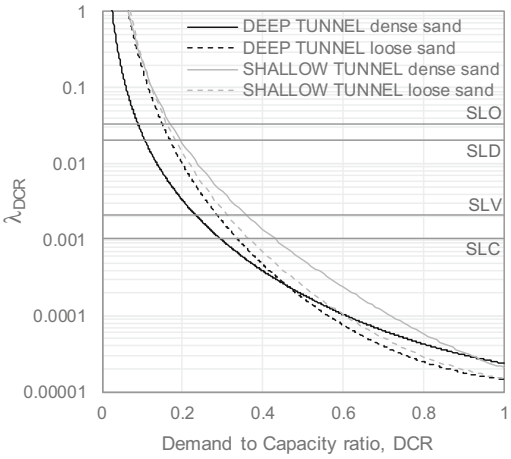

Fig. 5. DCR hazard curve of shallow and deep tunnel in dry and loose sand located in Naples.

6 Conclusions

The final goal of seismic performance-based design is the estimation of the expected losses caused by earthquakes. Losses need to be evaluated after the joint analysis of hazard and fragility, expressed by the DCR hazard curves. For this reason, DCR hazard curves are expected to become a widespread tool in the seismic design, at least, of new buildings, since they allow for immediate checking of the desired performance as well as for "exhaustive" individuation of the site-specific structural response. Moreover, their predictions can be applied to preliminary assess the seismic risk of built heritage, by considering the mobilization factor at which the existing structure and/or infrastructure was designed. This study is only a preliminary computation of the DCR hazard curves of some underground tunnel sections located in Naples. Further investigations are necessary to classify the performance parameters, define the limit states and identify the most efficient procedure of application to geotechnical engineering.

References

Andreotti G, Lai C (2014) Seismic vulnerability of deep tunnels: numerical modelling for a fully nonlinear dynamic analysis. In: Proceedings of the 2nd European conference on earthquake engineering and seismology

Argyroudis A, Pitilakis K (2012) Seismic fragility curves of shallow tunnels in alluvional deposits. Soil Dyn Earthquake Eng 35:1–12

Argyroudis S, Tsinidis G, Gatti F, Pitilakis K (2017) Effects of SSI and lining corrosion on the seismic vulnerability of shallow circular tunnels. Soil Dyn Earthquake Eng 98:244–256

de Silva F, Scotto di Santolo A (2018) Probabilistic performance-based approaches to the static and seismic assessment of rock cavities. Int J Rock Mech Min Sci 112:354–368

de Silva F, Fabozzi S, Nikitas N, Bilotta E, Fuentes R (2019) Soil-tunnel interaction under earthquake. In: Geotechnique symposium in print 2019 – linear infrastructure (under review)

Fabozzi S, Bilotta E, Lanzano G (2017) A numerical study on seismic vulnerability of tunnel linings. In: Proceedings of third international conference on performance-based design in earthquake, Vancouver (Canada)

Hardin BO (1978) The nature of stress-strain behaviour for soils. In: Proceedings of the ASCE Geotechnical Engineering Division Specialty Conference, ASCE, Pasadena, pp 3–90

Jalayer F, Cornell CA (2009) Alternative nonlinear demand estimation methods for probability-based seismic assessments. Earthquake Eng Struct Dynam 38(8):951–972

Kiani M, Ghalandarzadeh A, Akhlaghi T, Ahmadi M (2016) Experimental evaluation of vulnerability for urban segmental tunnels subjected to normal surface faulting. Soil Dyn Earthquake Eng 89:28–37

Kramer SL (2008) Performance-based earthquake engineering: opportunities and implications for geotechnical engineering practice. In: 4th congress on geotechnical earthquake engineering and soil dynamics, Sacramento, CA, United States, May 18–22

Kramer SL (2014) Performance-based design methodologies for geotechnical earthquake engineering. Bull Earthquake Eng 12(3):1049–1070

Kuhlemeyer RL, Lysmer J (1973) Finite element method accuracy for wave propagation problems. J Soil Mech Found Div 99:421–427

Iervolino I, Spillatura A, Buzzurro P (2017) RINTC PROJECT: assessing the (implicit) seismic risk of code-conforming structures in Italy. In: COMPDYN 2017 6th ECCOMAS thematic conference on computational methods in structural dynamics and earthquake engineering, Rhodes Island, Greece, 15–17 June

Itasca (2011) FLAC 7.0 – fast Lagrangian analysis of continua – user's guide. Itasca Consulting Group, Minneapolis

Miano A, Jalayer F, Ebrahimian H, Prota A (2018) Cloud to IDA: efficient fragility assessment with limited scaling. Earthquake Eng Struct Dyn 27(4):1124–1147

Pitilakis K, Crowley H, Kaynia A (Eds) (2014) SYNER-G: Typology definition and fragility functions for physical elements at seismic risk: buildings, lifelines, transportation networks and critical facilities. Geotechnical, geological and earthquake engineering, vol 27. Springer, the Netherlands

Salmon M, Wang J, Jones D, Wu, Ch (2003) Fragility formulation for the BART system. In: Proceedings of the 6th US conference of lifeline earthquake engineering, TCLEE, Long Beach, 10–13 Aug 2003

Seed HB, Idriss IM (1970) Soil moduli and damping factors for dynamic response analyses, Technical Report EERRC-70-10, University of California, Berkeley